Structure and Properties of Nanocomposites Based on Nylon-11 and -12 Compared with Those Based on Nylon-6

T. D. Fornes and D. R. Paul*

Department of Chemical Engineering and Texas Materials Institute, The University of Texas at Austin, Austin, Texas 78712

Received June 22, 2004; Revised Manuscript Received July 27, 2004

ABSTRACT: An in-depth analysis was made on the effect of polyamide repeat structure on the morphology and mechanical properties of nanocomposites based on nylon-6, nylon-11, and nylon-12. Special care was taken to make comparisons under fixed thermal and rheological conditions. Increasing the aliphatic content relative to nylon-6 results in a decrease in the extent of organoclay exfoliation as revealed by transmission electron photomicrographs. The extent of platelet separation as judged by low-angle X-ray scattering is more complicated for nylon-11 and -12 nanocomposites than those based on nylon-6 due the presence of crystalline peaks associated with the polyamide matrix. An "exfoliation index" is used to compare stiffness effects observed in the different nanocomposites due to the large difference in the modulus of nylon-6 as compared to nylon-11 and -12. Interestingly, the exfoliation efficiency parallels morphological trends in that nylon-6 exhibits higher efficiencies than the more aliphatic nylon-11 and -12 based nanocomposites. Izod impact strengths for nanocomposites based on nylon-6 are virtually insensitive to clay content for the concentrations examined, while those for nanocomposites based on nylon-11 and -12 decreases dramatically with increasing clay concentration; this behavior is believed to stem primarily from the location of the Izod ductile-to-brittle transition temperature relative to the ambient testing temperature for the three different types of nanocomposites. In addition to repeat structure investigations, a cursory examination of the effect of nylon-6 end groups was performed.

Introduction

Layered silicates can impart high levels of reinforcement to polymers at very low concentrations which makes them attractive for replacement of conventional fillers. Well-exfoliated nanocomposites based on polyamides can be made by in situ polymerization[1,2] and melt processing techniques.[3−5] The latter has received much attention due to its compatibility with existing polymer processing techniques and the ease with which the formulation can be manipulated. To date, however, commercialization of nanocomposites has been limited by an insufficient understanding of how to achieve high levels of exfoliation.

Nanocomposites have been formed by melt processing from a wide variety of polymers. Interestingly, those based on nylon-6 seem to have the highest level of exfoliation; in fact, nylon-6 appears to lead to better dispersion than is found for nylon-6,6 despite their similarity in chemical structure.[6] It is important to understand why nylon-6 is capable of producing such well-exfoliated nanocomposites. We have taken a two pronged approach to evaluate how component structure affects nanocomposite morphology and physical properties. The first involves understanding how the chemical structure of the alkylammonium surfactants used to make an organoclay from montmorillonite influences exfoliation in nylon-6. Recent studies have shown that in order to achieve well-exfoliated morphologies and subsequently superior mechanical properties, it is necessary to adjust the surfactant structure to provide the polar polymer access to the montmorillonite surface which also reduces platelet−platelet interactions.[7] The second involves understanding how polyamide structure, viz., degree of polymerization, molecular weight, repeat unit structure, and end groups, affects organoclay exfoliation and, ultimately, mechanical properties. Previous studies in our laboratory indicated that the molecular weight of the nylon-6 plays a key role in producing well-exfoliated nanocomposites; high molecular weight materials lead to much better exfoliation than low molecular weight materials.[8−10] It is believed that this stems from the higher melt viscosity caused by the high molecular weight and, consequently, the larger shear stresses on the organoclay particle during melt processing.

The chemical structure of the polymer affects its interaction with both the clay surface and the organic modifier which influences exfoliation during melt processing. Clearly, the extent and nature of the polarity of the polymer repeat unit are important. For example, a nonpolar polymer like polypropylene has a less repulsive interaction with alkyl tails on the surfactant than does nylon-6, but it has a much lower affinity for the clay itself; as a result, organoclays do not disperse well in polypropylene. However, dispersion of organoclay in polypropylene can be significantly improved by grafting maleic anhydride to the polypropylene to act as a "compatibilizer".[11−13] The very polar nature of the amide linkages appear to be a key reason why organoclays are easily delaminated by nylon-6.

In addition to repeat structure, end groups conceivably could be of importance in the formation of well-exfoliated nanocomposites. The carboxylic acid and amine end groups of polyamides have been used to strengthen the interface and control the morphology in both glass fiber composites and their blends with other polymers. Numerous investigations conducted in this laboratory and elsewhere[14−20] have demonstrated the role of amine end group concentration and configuration for controlling the size and dispersion of functionalized

* Corresponding author: Tel 512-471-5392; fax 512-471-0542; e-mail drp@che.utexas.edu.

10.1021/ma048757o CCC: $27.50
Published on Web 09/09/2004

Table 1. Materials Used in This Study

material [designation used here]	commercial designation	comments/specifications	supplier
		Polymers	
nylon-6 [PA-6]	Capron B135WP	high viscosity grade Brabender torque (N·m) = 10.9[a] $\bar{M}_n$ = 31100 PDI[b] = ~2 end group concn (μequiv/g) [COOH] = 28.8 [NH_2] = 34.5	Honeywell
nylon-6 [PA-6-Capped]	experimental	high viscosity grade Brabender torque (N·m) = 10.4[a] $\bar{M}_n$ = N/A[c] PDI[b] = N/A[c] end group concn (μequiv/g) [COOH] = 30.8 [NH_2] = 8.5	BASF
nylon-11 [PA-11]	Rilsan BENSO TL	medium to high viscosity grade Brabender torque (N·m) = 12.6[a] $\bar{M}_n$ = 17200 PDI[b] = ~2	Atofina
nylon-12 [PA-12]	Rilsan AENSO TL	medium to high viscosity grade Brabender torque (N·m) = 12.3[a] $\bar{M}_n$ = 16000 PDI[b] = ~2	Atofina
		Organoclays	
trimethyl hydrogenated-tallow ammonium montmorillonite [$M_3(HT)_1$][b]	experimental	95 MER[e] % LOI = 29.6 wt %[e] d_{001} spacing = 1.80 nm	Southern Clay Products
bis(2-hydroxyethyl)methyl rapeseed ammonium montmorillonite [$(HE)_1M_1R_1$][b]	experimental	95 MER[e] % LOI = 34.1 wt %[e] d_{001} spacing = 1.80 nm	Southern Clay Products

[a] Brabender torques correspond to steady-state values measured at 10 min and beyond at a temperature of 240 °C. [b] PDI represents the molecular weight polydispersity index. [c] N/A = not available. [d] The substituents on the quaternary ammonium compound used to form the organoclays are identified in the following shorthand notation: HT = hydrogenated tallow, R = rapeseed, HE = 2-hydroxyethyl, and M = methyl. Tallow and rapeseed are natural products composed predominantly of unsaturated C_{18} and C_{22} alkyl chains. [e] The milliequivalent ratio (MER) indicates the number of milliequivalents of amine salt used per 100 g of clay during the cationic exchange reaction with sodium montmorillonite. The loss on ignition (LOI) is the loss of mass per gram of dry organoclay when heated to 900 °C for 45 min. The basal spacing corresponds to the characteristic Bragg reflection peak (d_{001}) obtained from a powder WAXS scan of the organoclay.

rubbers (typically grafted with maleic anhydride) and the subsequent generation of super-tough materials. The amine−anhydride chemical reaction represents one extreme in the spectrum of potential interactions. In the case of nanocomposites, the amine end groups, as well as the carboxylic acid units, are capable of physically interacting with the face of the clay.[21] In addition, when protonated, the amine unit may participate in ion exchange with the absorbed cations; however, this would require an acidic environment not likely to exist in the melt state. Of course, the role of end group interactions with the clay surface are strongly modulated by their low concentration of typical molecular weights.

Comparison of the effects of polymer repeat unit structure or end group effects on exfoliation is not a trivial experimental task. It is not possible to deduce relatively subtle effects from the reports in the literature due to differences in materials and processing conditions, e.g., polymer molecular weight and organoclay type, extruder type, screw configuration, extrusion temperature, screw speed, etc. An unambiguous comparison requires careful selection of materials and fabrication under the same melt processing conditions; the present work attempts to do this.

The aim of this paper is to evaluate the effects of polyamide structure on the morphology and physical properties of melt-processed nanocomposites. An in-depth analysis is made of the influence of polyamide repeat structure on the level of clay exfoliation and mechanical property enhancement by comparing nanocomposites based on nylon-6, nylon-11, and nylon-12, whereas, a cursor examination is made to address the role of nylon-6 end groups. Special care is taken to make each nanocomposite comparisons at fixed thermal and rheological conditions.

Experimental Section

Materials. Table 1 lists the materials used in this work. These polymers were selected from a series of commercial and experimental materials because their rheological behavior are similar to that of the PA-6 employed in prior studies[8,9] at the appropriate temperature and shear during extrusion compounding conditions. To mimic the environment of the extruder, the melt rheology of the materials was characterized using a Brabender torque rheometer equipped with a 60 mL mixing bowl filled to capacity, operating at 60 rpm and 240 °C. Polyamides having torques (see Table 1) comparable to that of the PA-6 were selected for this study; the torques reported are steady-state values obtained at 10 min and beyond. Details of the techniques used to determine molecular weight information for the PA-6, PA-11, and PA-12 materials can be found in the literature.[22−24] The material designated as PA-6-Capped is an experimental grade of nylon-6 with a reduced content of amine end groups.

The organoclays used in this study were formed by a cation exchange reaction between sodium montmorillonite (CEC = 92 mequiv/100 g clay) and quaternary alkylammonium chlorides. A simple nomenclature system is used to describe the

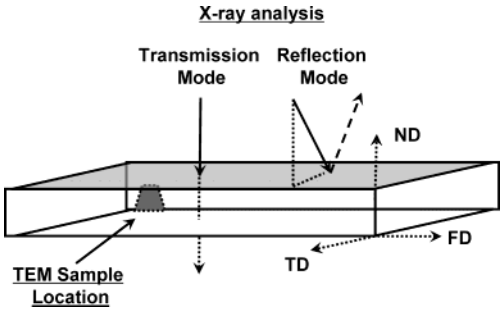

Figure 1. Illustration of incident X-ray beam in reflection and transmission and TEM sampling location in relation to the transverse (TD), flow (FD), and normal directions (ND) of an injection-molded bar.

substituents on the nitrogen of the organic modifier. The symbol M represents methyl, HE represents 2-hydroxy-ethyl, and T and R represent units derived from the natural products tallow and rapeseed, respectively, each consisting of a distribution of saturated and unsaturated hydrocarbons. The hydrogenated form of T, designated here as HT, still contains a small amount of unsaturation. The organoclay $(HE)_2M_1R_1$ (Table 1) was chosen on the basis of previous polymer structure−nanocomposite property investigations, in particular, those regarding the effect of nylon-6 matrix molecular weight. The organoclay $M_3(HT)_1$ was chosen because of its ability to readily delaminate in PA-6.[7,25]

Melt-Processing. Nanocomposites were formed by extruding mixtures of organoclay and polymer pellets using a Haake corotating twin screw extruder (diameter = 30.5 mm, L/D = 10) operating at a barrel temperature of at 240 °C, a feed rate of ∼1 kg/h, and screw speed of 280 rpm. The amount of MMT in each nanocomposite was verified by placing predried pellets in a furnace at 900 °C for 45 min and measuring the remaining MMT ash. A correction for loss of structural water that occurred during incineration is included in the calculation.[7] Nanocomposite pellets were injection-molded into standard 3.18 mm thick tensile (ASTM D638) and Izod bars (ASTM D256) using an Arburg Allrounder 305-210-700 injection-molding machine at an injection pressure = 70 bar, holding pressure = 35 bar, a barrel temperature = 260 °C, and a molding temperature = 80 °C. Prior to each melt-processing step, all polyamide materials were dried at 80 °C under vacuum for a minimum of 12 h.

X-ray Analyses. Wide-angle X-ray scattering (WAXS) experiments were conducted primarily in reflection mode with a Scintag XDS 2000 diffractometer using Cu K_α radiation source (λ = 0.154 nm), set at a scan rate = 1°/min, a voltage = 45 kV, and current = 40 mA. The width of the source-side slits used were 4 mm for the scattering slit (closest to the sample) and 2 mm for the divergence slit (closest to the source), while the width of the detector-side slits used were 0.5 mm for the scattering slit (closest to the sample) and 0.2 mm for the receiving slit (closest to the detector). Scans were performed on organoclay powder and injection molded nanocomposites (Izod bars); the bars were orientated such that the incident beam reflected off the plane comprised of the transverse (TD) and flow directions (FD), as indicated in Figure 1. For selected nylon-12 materials, X-ray analyses were executed in transmission mode using a Rigaku diffractometer (voltage = 50 kV and current = 40 mA) equipped with a precession camera having a sample to imaging film distance of 65 cm and a Cu K_α radiation source (λ = 0.154 nm). To have an acceptable level of transmitted intensity, the top half of each Izod bar was milled off prior to analyzing. Samples were oriented such that the incident beam was parallel to the normal of the TD−FD plane, as shown in Figure 1, and irradiated for 10−15 min. The resulting image on the film was developed, scanned into a computer, and analyzed using FIT2D software. The scattering properties of the same nylon-12 samples were further examined in transmission in the melt state to remove any low-angle crystalline reflections associated with the nylon-12 using a Molecular Systems SAXS unit (voltage = 80 kV and current = 75 mA) equipped with a Cu K_α radiation source (λ = 0.154 nm) and a solid state detector located 35.0 cm from the sample. The size of the beam at the sample was approximately 0.2 mm in height by 5 mm in width. Samples were sandwiched between aluminum foil, placed in an open stainless steel assembly, and heated to 210 °C. X-rays were collected under vacuum for 45 min at room temperature prior to melting, in the melt state, and at room temperature following slow cooling from the melt.

Transmission Electron Microscopy. Samples for TEM analysis were extracted from the central cross section of an Izod bar in the FD-ND plane and viewed along the TD direction, as indicated in Figure 1. Ultrathin sections approximately 50 nm in thickness were cryogenically cut with a diamond knife at a temperature of −40 °C using a Reichert-Jung Ultracut E microtome. Sections were placed on 300 mesh copper grids and subsequently examined at an accelerating voltage of 120 kV using a JEOL 2010F TEM equipped with a field emission gun.

Mechanical Testing. Stress−strain analyses were conducted in tension on injection-molded tensile bars (ASTM 638D) as previously described.[8,9] Modulus and yield strength were measured using a crosshead speed of 0.51 cm/min, whereas elongation at break was determined at a speed of 5.1 cm/min. Notched Izod impact tests were conducted at room temperature using a TMI Izod tester according to ASTM D256. Standard deviations were typically 4% for modulus, 2% for yield strength, and 8% for Izod impact strength, while elongation showed larger variations, i.e., between 5 and 30%.

Results

Nanocomposite Morphology. Figure 2 shows X-ray scans at low 2θ values for nanocomposites formed from PA-6, PA-11, and PA-12 and the organoclay, $M_3(HT)_1$. Table 2 lists the location of each peak observed at both low and high angles and corresponding *d*-spacings. Nanocomposites based on PA-6 exhibit smooth scattering profiles at low angles (see Figure 2a), absent of any basal reflections, which is indicative of disruption of the once ordered organoclay. Increasing the number of methylene units in the polyamide's repeat structure by five or six, however, results in significant changes in low-angle scattering, evident in Figure 2b,c. At first glance, these results imply poor exfoliation of the organoclay; however, closer examination of the plots suggest differently. The nanocomposites display reflections at significantly higher 2θ values (lower *d* spacings) than that of the pure organoclay; i.e., nanocomposites based on PA-11 and PA-12 display reflections at ∼5.9° of 2θ (∼1.52 nm) and ∼6.1° 2θ (∼1.45 nm), respectively, while the basal spacing of the pure organoclay is 1.80 nm. In fact, these peaks are believed to be associated with the crystalline phase of the polymer matrix. A number of crystallographic studies on pure nylon-11 and -12 have reported reflections at or near 1.45 nm,[26−32] which have been associated with the crystalline phase of the α- and β-forms in nylon-11 and γ-form in nylon-12. Moreover, nanocomposite studies by Reichert et al.[33] and McNally et al.[34] report similar observations at low angles for nylon-12 nanocomposites formed by in situ polymerization and melt processing techniques. Interestingly, the pure PA-11 and PA-12 materials lack distinct low-angles reflections as observed in their respective nanocomposites. This difference may stem from changes in the orientation of crystallites relative to the incident X-ray beam due to the presence of the clay or other causes.

Wide-angle X-ray data provide better insight into the different polyamide crystalline structures for each of the

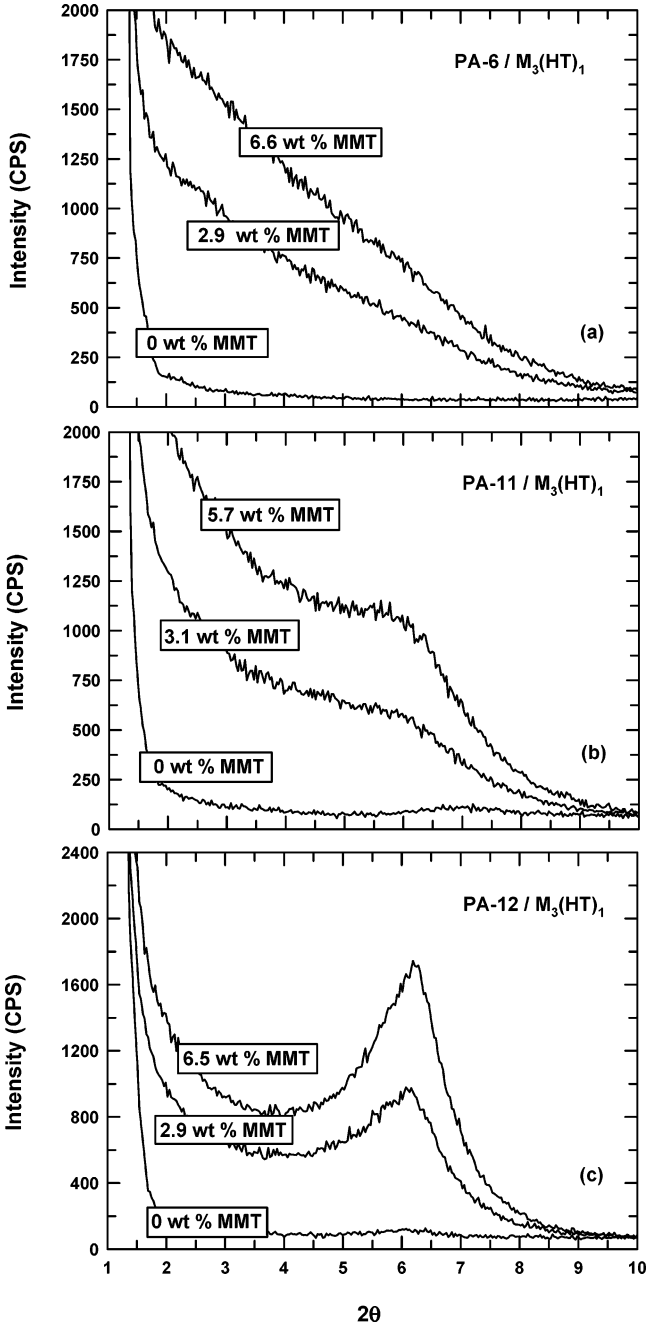

Figure 2. X-ray reflection results at low 2θ values for pure and nanocomposite samples based on $M_3(HT)_1$ organoclay and (a) PA-6, (b) PA-11, and (c) PA-12.

nanocomposites. However, before discussing these results, the differences between the various crystalline forms of even *n*-nylons, such as nylon-4, nylon-6, nylon-8, etc., and odd *n*-nylons such as nylon-5, nylon-7, nylon-9, etc., should be briefly explained; a more in-depth overview can be found in the work of Aharoni.[35] The most significant factor controlling the crystalline form produced in linear aliphatic polyamides is that all possible hydrogen bonds are completely satisfied.[35] To meet this criterion, chains will adopt a fully extended configuration (α-form) or a slightly twisted configuration (γ-form) and will orient in a parallel or antiparallel fashion, depending upon the number of CH_2 groups in the repeat structure. In the fully extended configuration or α-form, hydrogen bonds occur between amides in the same plane as the CH_2 zig-zags, forming one large

Table 2. X-ray Peak Locations and Corresponding *d* Spacings of $M_3(HT)_1$ Organoclay, PA-6, PA-11, and PA-12, and Nanocomposites Made from These Materials

material	2θ (deg)	*d*-spacing (nm)
organoclay		
$M_3(HT)_1$	4.9	1.80
HMW PA-6/$M_3(HT)_1$		
0.0 wt % MMT	21.2	0.42
2.9 wt % MMT	21.1	0.42
6.6 wt % MMT	21.2	0.42
PA-11/$M_3(HT)_1$		
0.0 wt % MMT	7.0, 20.8, 22.0[a]	0.26, 0.43, 0.40
3.1 wt % MMT	5.9, 20.4, 23.1[a]	1.50, 0.43, 0.38
5.7 wt % MMT	5.9, 20.4, 23.1[a]	1.50, 0.43, 0.38
PA-12/$M_3(HT)_1$		
0.0 wt % MMT	6.2, 21.3	1.42, 0.42
2.9 wt % MMT	6.2, 19.5[a], 21.2, 25.4	1.42, 0.45, 0.42, 0.35
6.5 wt % MMT	6.2, 19.5[a], 21.3, 25.6	1.42, 0.45, 0.42, 0.35

[a] Small shoulder.

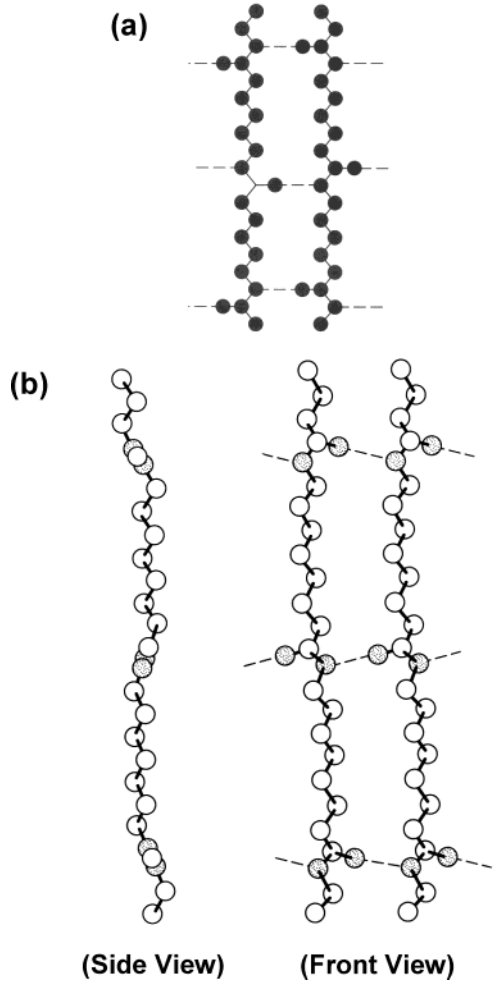

Figure 3. Chains in the (a) fully extended configuration of the α-crystalline form and the (b) twisted configuration of the γ-crystalline form of even *n*-nylons. The graphics in this figure were reproduced from the work of Aharoni[32] with permission.

molecular sheet. This configuration is also associated with the β-form. The only difference in the α- and β-forms is the that in the α-form the molecular sheets are alternatively staggered up and down, whereas in the β-form, the sheets are shifted in one direction.[35] In the twisted configuration or γ-form, amide groups twist ~60° out of the plane of the molecular sheet. Figure 3 illustrates the two types of chain configuration for even *n*-nylons.[35] Complete consummation of hydrogen bonds

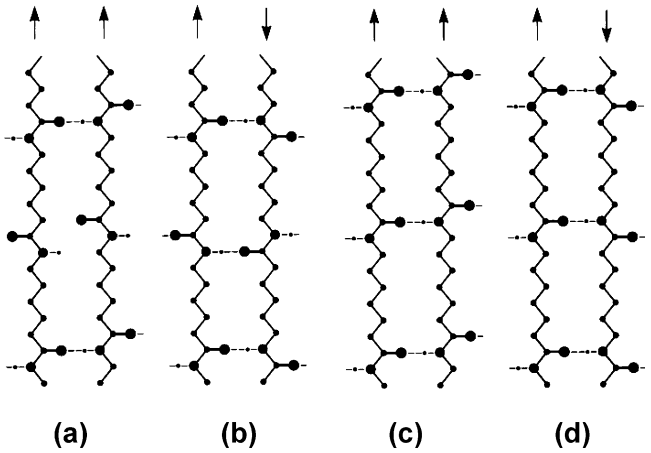

Figure 4. Relationships between chain orientation in the full extended configuration and the even or odd character of *n*-nylons. Even *n*-nylons (a, b) consummate all possible hydrogen bonds only in the antiparallel (b) orientation and not in the parallel (a) alignment. Odd *n*-nylons may be aligned in parallel (c) or antiparallel (b) orientation with full consummation of all possible hydrogen bonds. The graphics in this figure were reproduced from the work of Aharoni[32] with permission.

in the fully extended configuration of even *n*-nylons occurs only when polymer chains are orientated antiparallel to one another rather than parallel; otherwise, only half of the bonds are made (see Figure 4a,b). For odd *n*-nylons, complete consummation in the extended configuration can occur regardless of whether the polymer chains are oriented parallel or antiparallel as illustrated in Figure 4c,d; this is due to the centrosymmetric nature of odd *n*-nylons.

Therefore, in nylon-6 and nylon-12, the α- and γ-forms occur when hydrogen bonding in the crystal takes place between parallel and antiparallel chains, respectively. In nylon-11, chains may be parallel or antiparallel in both crystalline forms. Nylon-6 has been known to produce either crystalline form, depending upon crystallization conditions. Nylon-11 and -12 are also capable of producing both forms; however, it is well documented that the more stable form in nylon-11 is the α-form, while the γ-form is the more stable form in nylon-12; see references given by Aharoni.[35]

Figure 5 shows wide-angle X-ray data for the three types of nanocomposites. Materials based on PA-6 exhibit a sharp peak at ∼21.2°, of 2θ which is characteristic of the γ-form of nylon-6[35−41] (see Figure 5a). Adding dispersed clay to nylon-6 enhances this peak. Interestingly, the intermediate concentration of MMT has a higher intensity than the nanocomposite containing 6.6 wt % MMT. This effect likely stems from more ordered, larger crystallites due to fewer polymer−silicate interactions in the samples of intermediate clay contents; a more in-depth discussion of the crystallization behavior observed in nylon-6 nanocomposites is available in a prior publication.[42]

Diffraction patterns for PA-11 and corresponding nanocomposites in Figure 5b show strong reflections at 20.4−20.8° of 2θ , while a less intense peak or shoulder is observed around 23.1°. The intensities of the peaks increase considerably with addition of clay, yet the nanocomposite with an intermediate clay content has the highest intensity, similar to what is observed in PA-6. The location of the peaks represents the α-form of nylon-11[27,28] (also see references within ref 35). Similarly, low-angle reflections occurring at 2θ = 5.9° for the nanocomposites (see Figure 2b), in addition to the minor hump at 2θ = ∼7.0° for pure PA-11, are associated with the α-form and the closely related β-form, as mentioned earlier. Similar observations with regard to crystal structure have been made by Liu et al.[43] in nylon-11 nanocomposites also formed by melt-processing.

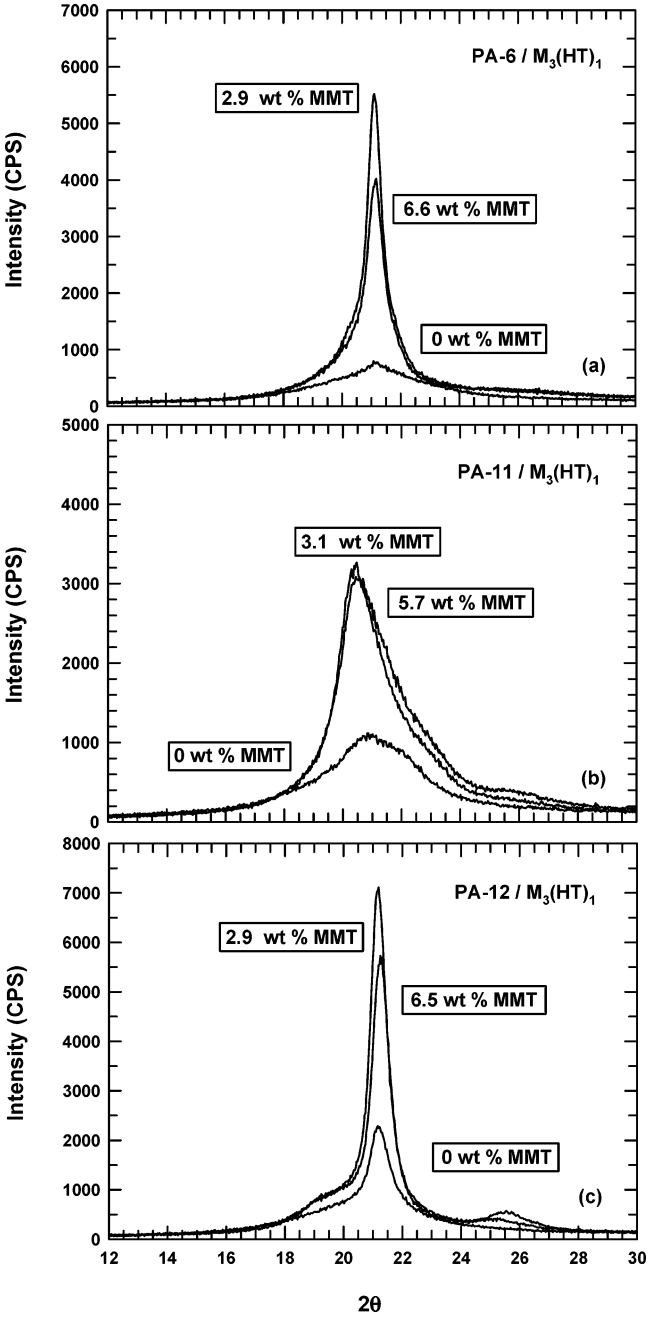

Figure 5. X-ray reflection results obtained at high 2θ values for pure and nanocomposite samples containing the $M_3(HT)_1$ organoclay contents shown for (a) PA-6, (b) PA-11, and (c) PA-12 as the matrix.

The diffraction patterns for PA-12 and corresponding nanocomposites shown in Figure 5c have a sharp peak at 21.2° of 2θ. As in the case of PA-6 and PA-11, the intensity of this peak increases with the addition of the clay; however, the intermediate clay concentration leads to the highest intensity. The *d* spacing of this peak (see Table 2) corresponds to the γ-form of nylon-12.[29−32] Likewise, the reflection at 2θ = 6.2° (*d* spacing = 1.42

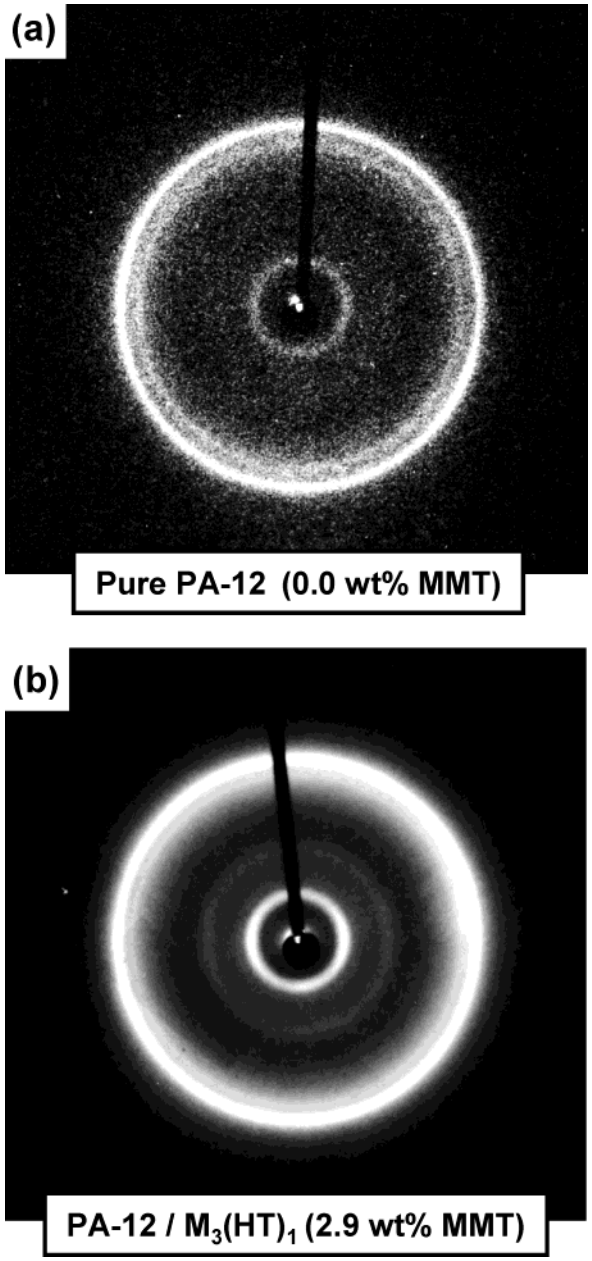

Figure 6. X-ray diffraction patterns obtained in transmission for (a) pure PA-12 and its corresponding (b) nanocomposite based on $M_3(HT)_1$ organoclay. The incident beam was oriented parallel to the normal of the FD-ND plane.

nm) shown in Figure 2c is indicative of the γ-form. As mentioned above, these X-ray results are in accord with the observations made by Reichert et al.[33] and McNally et al.[34] for nylon-12 nanocomposites formed by in situ polymerization and melt-processing techniques, respectively.

It was of interest to further examine the nature of the diffraction behavior of the nanocomposite materials to ensure that low-angle reflections indeed correspond to crystalline polymer and not unexfoliated clay. A series of X-ray experiments were conducted on selected PA-12 materials in transmission to gather information on the entire sample, unlike in reflection, where just the outer surface is probed. Figure 6 shows the diffraction patterns acquired in transmission for injection-molded PA-12 materials with and without clay. Both patterns exhibit rings at low and high angles; note that the inner ring in the nanocomposite sample (see Figure 6b)

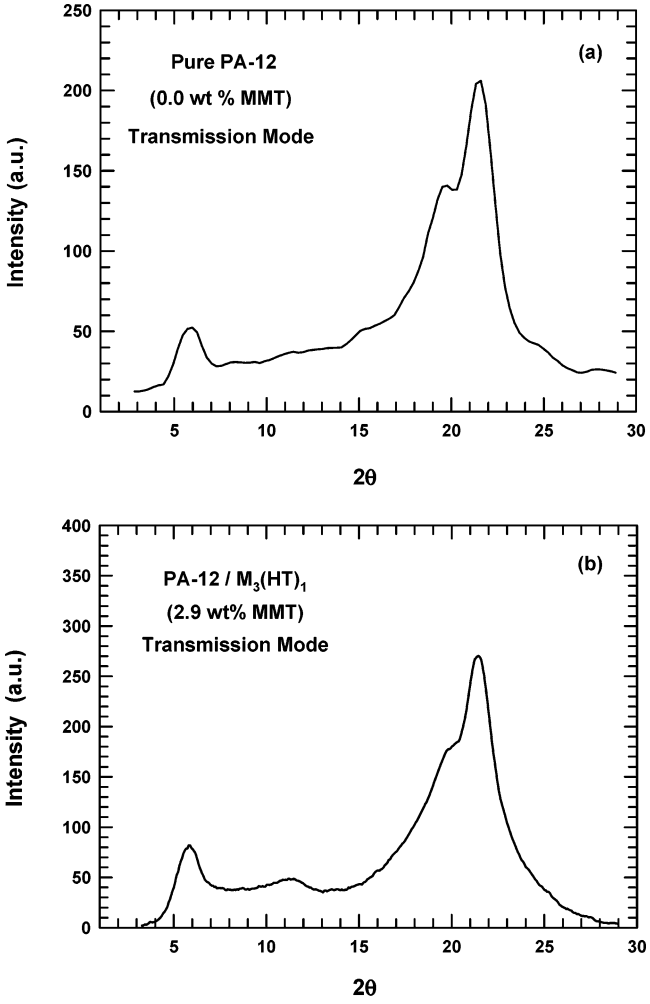

Figure 7. Intensity vs 2θ plots obtained from 2D integration of diffraction patterns shown in Figure 6 for (a) pure PA-12 and (b) its nanocomposite formed from the organoclay $M_3(HT)_1$.

broadens and intensifies along the lateral edges, which is suggestive of some ordering, whereas the inner ring in the pure PA-12 sample is isotropic (see Figure 6a). Performing a 2-D integration of the patterns yields a more quantitative description of diffraction in terms of intensity vs 2θ, as seen in Figure 7. The plots for both materials are nearly identical in shape, displaying peaks at $2\theta \sim 6.1°$ and 21.4°, corresponding to reflections of different crystallographic planes of the γ-crystalline form of nylon-12. Interestingly, the ratio of intensities of the low-angle peak to that of the high-angle peak for the nanocomposite is equivalent to the corresponding ratio for the pure PA-12, which further supports the belief that the low-angle reflection for the nanocomposite contains no contributions from unexfoliated clay platelets. Direct evidence for this premise is given in Figure 8, which shows the nanocomposite X-ray patterns in the low-angle region obtained at room temperature prior to melting, in the melt state, and at room temperature after cooling from the melt state. Prior to melting, an intense anisotropic ring ($2\theta \cong 6.1°$) is present which suggests some degree of structural orientation (see Figure 8a). Heating the sample well above its melting point causes the low-angle ring to completely disappear, resulting in an entirely diffuse pattern (see Figure 8b); this indicates that the low-angle reflection in Figure 2c is caused by the crystalline polymer matrix

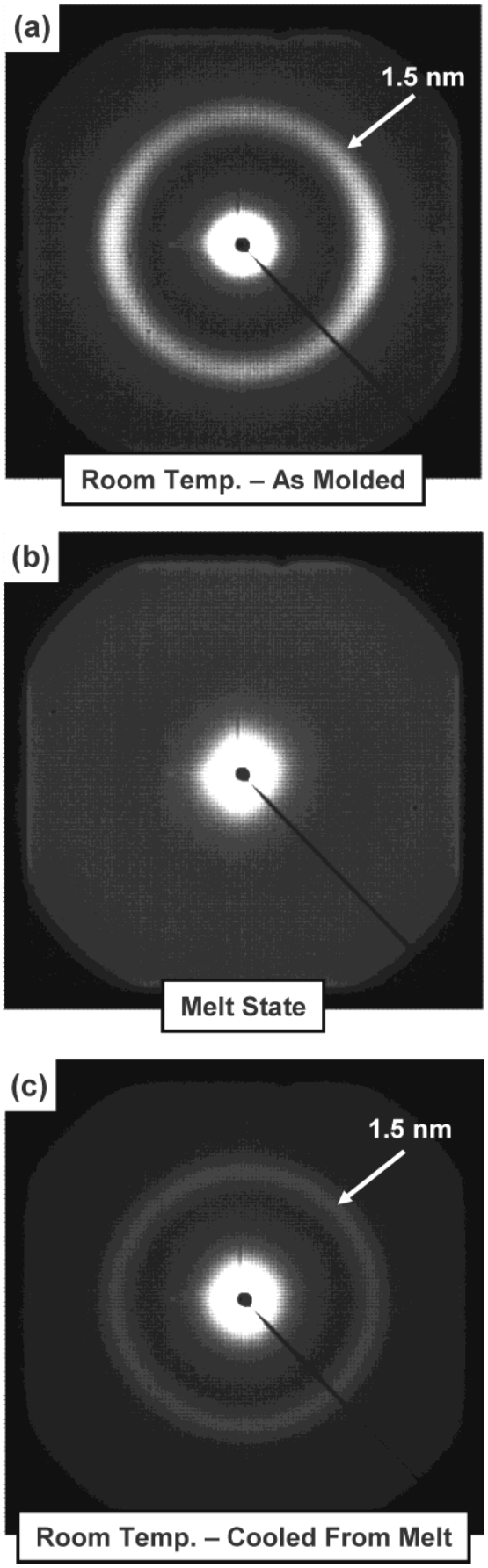

Figure 8. Small-angle X-ray patterns for PA-12/$M_3(HT)_1$ nanocomposites obtained (a) at room temperature prior to melting, (b) in the melt state (T = 210 °C), and (c) at room temperature following cooling from the melt.

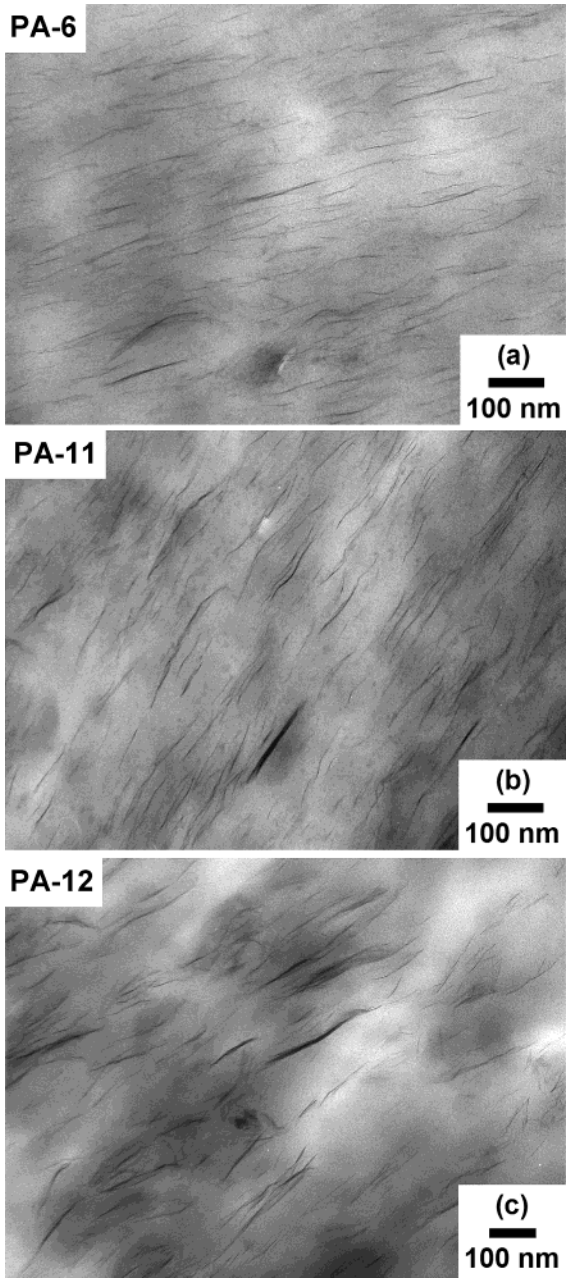

Figure 9. TEM photomicrographs of nanocomposites containing ~3 wt % MMT based on $M_3(HT)_1$ organoclay and (a) PA-6, (b) PA-11, and (c) PA-12 as the matrix.

rather than unexfoliated clay. Moreover, the diffuse image in Figure 8b implies that the organoclay is delaminated to an extent that interparticle distances are not detectable by X-rays. Last, slowly cooling the sample down to room temperature causes the crystalline peak to reappear, as seen in Figure 8c; however, the ring is completely uniform, indicative of an isotropic state. In total, the above discussion emphasizes the care that must be taken to avoid overinterpretation of X-ray scattering behavior of nanocomposites. In many instances, X-ray scans alone fail to give the full picture of the state of clay dispersion as seen here, but this is a somewhat special case.

The TEM photomicrographs in Figure 9 provide more conclusive evidence of the extent of clay dispersion and support the interpretation of the X-ray results given above. Nanocomposites based on PA-6 (see Figure 9a) have a well-exfoliated morphology consisting predomi-

Table 3. Mechanical Property Data for $M_3(HT)_1$ Nanocomposites Based on Nylon-6, -11, and -12

wt % MMT	modulus (GPa)	yield strength (MPa)	elongation at yield[a] (%)	elongation at break[b] (%)	Izod impact strength (J/m)
			PA-6/$M_3(HT)_1$ Nanocomposites		
0.0	2.75	69.7	4.0	129	43.9
1.5	3.51	84.0	3.4	NA	34.7
2.9	4.23	85.2	2.9	31	34.4
4.6	4.71	90.7	2.8	16	37.0
6.6	5.18	69.7	NA[c]	3.6	36.5
			PA-11/$M_3(HT)_1$ Nanocomposites		
0.0	1.30	41.3	24.3	312	116.2
1.8	1.60	44.3	27.0	251	75.5
3.1	1.93	47.1	23.4	264	38.0
4.0	2.04	48.9	20.5	206	33.4
5.7	2.33	51.4	14.8	65	31.0
			PA-12/$M_3(HT)_1$ Nanocomposites		
0.0	1.49	40.9	13.6	286	161.1
1.7	1.79	44.9	12.6	245	106.9
2.9	2.03	46.7	11.2	246	78.2
4.4	2.32	48.4	9.4	131	69.9
6.5	2.69	50.5	7.9	62	40.0

[a] Elongation at yield values for compositions based on PA-11 and P-12 were determined using crosshead deflection. [b] Measured at a crosshead head speed = 5.1 cm/min. [c] Sample broke prior to yielding.

nantly of individual platelets dispersed uniformly throughout the polymer matrix which are highly aligned along the direction of flow; these results agree with previous TEM observations on injection-molded nanocomposites.[25] Nanocomposites based on PA-11 and PA-12 matrices (see Figure 9b,c) also exhibit highly exfoliated and aligned structures; however, the extent of platelet delamination is noticeably less, particularly for the PA-12 nanocomposite. Close examination of photomicrographs like that of Figure 9c reveals the existence of a large fraction of particles compromised of multiple platelets. In addition, the average spacing between particles is greater than what is observed in the PA-6, which is another indication of less exfoliation. The degree of platelet alignment also appears to be less in the nylon-12 matrix, and to a somewhat smaller extent in the nylon-11 matrix, compared to that for nylon-6; this may be a consequence of less exfoliation, since particles of having smaller aspect ratios are less likely to align unidirectionally than larger aspect ratio particles.

Mechanical Properties. Enhancements in mechanical properties associated with the addition of the clay provide another means of assessing the effects of polyamide repeat structure on the extent of exfoliation in polyamide nanocomposites. However, before discussing this point, it is important to highlight the key differences in stress−strain behavior observed in nylon-6, -11, and -12 in the absence of clay illustrated in Figure 10. Nylon-6 inherently has a higher modulus and yield strength than nylon-11 or -12. The yield point reported for these materials is defined as the highest stress at which $d\sigma/d\epsilon = 0$. The postyield deformation behavior is also sizably different among these materials; i.e., the onset of necking and elongation at break for nylon-6 is considerably less than for nylon-11 or nylon-12. These tensile parameters will be altered to different degrees when clay is dispersed in each of these polymer matrices because of differences in the degree of exfoliation and other composite effects relating to the intrinsic matrix properties; Table 3 documents the effects of adding clay to PA-6, PA-11, and PA-12 on their mechanical properties.

It is recognized that the degree of modulus enhancement experienced in polymer−clay nanocomposites is

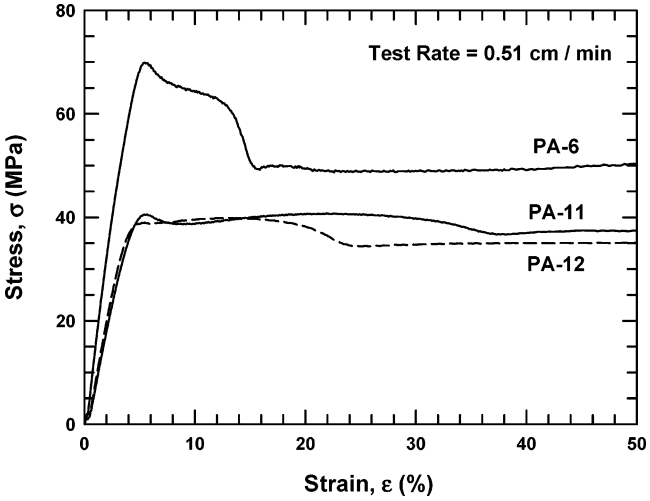

Figure 10. Stress−strain behavior of pure PA-6, PA-11, and PA-12 measured at a crosshead speed of 0.51 cm/min.

proportional to the aspect ratio of the dispersed clay particle, which is directly related to the extent of clay exfoliation. However, a point often overlooked is that low-modulus matrices offer greater potential for reinforcement per mass filler than high-modulus matrices for a given filler aspect ratio due to the larger ratio of filler modulus to matrix moduli. Furthermore, the greater this ratio is, the more sensitive the nanocomposite modulus is to the aspect ratio of the filler; in the limit of an infinite aspect ratio, the composite modulus must follow a simple additivity rule, i.e., $E = \phi_1 E_1 + \phi_2 E_2$. This point is illustrated in Figure 11 where the relative modulus of the composite matrix for a given concentration of MMT is plotted vs the modulus of the polymer matrix as calculated using the Halpin−Tsai theory;[44,45] the assumptions used to generate each curve are that the MMT filler is perfectly exfoliated, aligned parallel to the applied stress, and has a modulus value equivalent to that of muscovite (178 GPa),[46,47] a mica-based layered silicate very similar in structure to MMT.[48] Thus, comparing the relative modulus of nanocomposites based on polymer matrices of drastically different stiffness to assess the extent of clay exfoliation can be misleading if this effect is not considered.

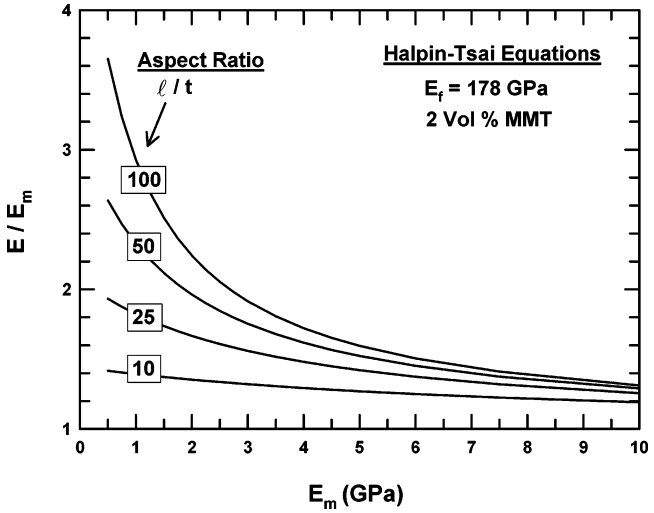

Figure 11. Relative stiffness of nanocomposites calculated using the Halpin−Tsai theory as a function the matrix modulus and filler aspect ratio for a constant MMT content.

To account for this issue in comparing results for the present nanocomposites, we use an "exfoliation efficiency" index as a means of evaluating the extent of exfoliation from stiffness properties. This index is defined as the modulus of the nanocomposite as measured experimentally divided by the modulus calculated from theory assuming exfoliation is perfect (for a fixed MMT content), i.e.

$$\text{exfoliation efficiency (wt \% MMT)} = \frac{E_{\text{expt}}}{E_{\text{theory}}} \quad (1)$$

The numerator corresponds to modulus data listed in Table 3, while the denominator in eq 1 is determined using the theory of Halpin−Tsai using the following assumptions: The filler is completely exfoliated and perfectly aligned along the direction of applied stress, i.e., the flow direction (see Figure 1). The aspect ratio of the individual platelets is taken to be $l/t = 97$, corresponding to a platelet length of 91 nm divided by the thickness of an individual platelet of 0.94 nm.[49] This length value represents the number-average length of MMT particles previously determined by a quantitative image analysis of TEM photomicrographs of well-exfoliated PA-6 nanocomposites.[10,49,50] It is further assumed that this length distribution is an inherent characteristic of the clay and is unaffected by the process of making the nanocomposite; future work will attempt to address this issue. Last, the number-average particle length, as opposed to weight-average length, is taken as the appropriate average to use based on the composite modeling studies by Hine et al.[51] that showed that the Halpin−Tsai theory provides a more accurate prediction of the moduli of glass fiber reinforced composites when the number-average aspect ratio is used.

Figure 12a shows a plot of exfoliation efficiency vs wt % MMT for the three types of nanocomposites; the plot of composite modulus vs wt % MMT is shown in Figure 12b for comparative purposes. Nanocomposites based on nylon-6 exhibit a near-perfect exfoliation efficiency, particularly at low clay concentrations, whereas those based on nylon-11 and -12 exhibit significantly lower efficiencies. Increasing the number of methylene units in the polyamide repeat from 5 to 10, i.e., nylon-6 vs nylon-11, results in the greatest effect, while going from

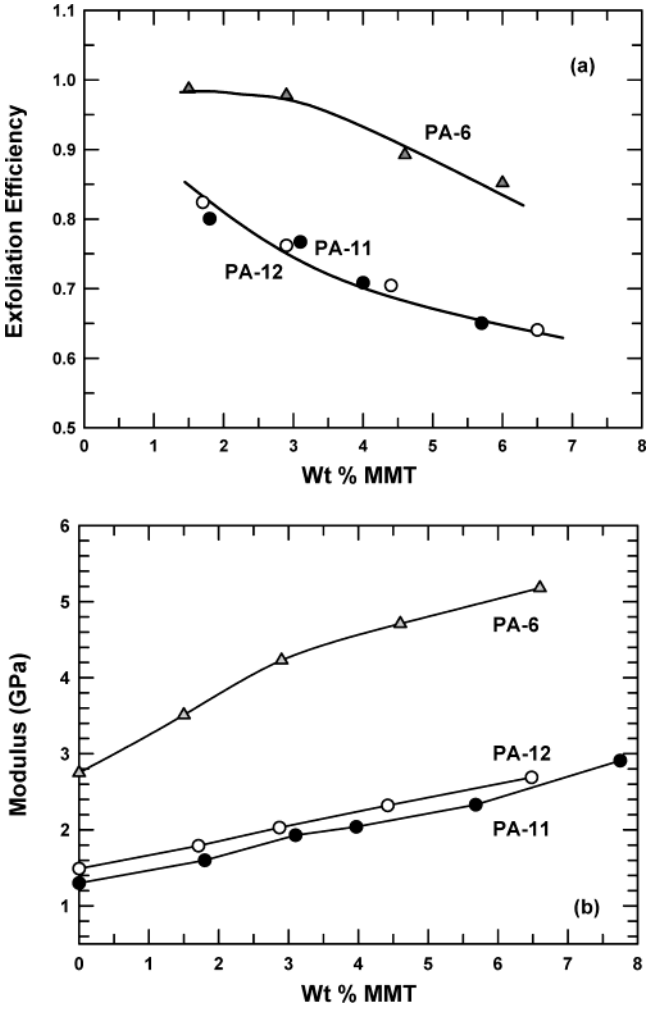

Figure 12. Effect of MMT content and polyamide repeat structure on (a) exfoliation efficiency, defined as the ratio the experiment modulus over the modulus calculated from the Halpin−Tsai theory assuming perfect exfoliation, and (b) the experimental modulus for nanocomposites based on PA-6, PA-11, and PA-12 and the organoclay $M_3(HT)_1$.

10 to 11 has little effect at all, which might be expected. Interestingly, exfoliation efficiency decreases with increasing clay concentration in all three polyamides. Such effects have been observed in a variety of other matrices such as epoxy,[52] ethylene vinyl acetate,[53] polypropylene,[54−56] styrene−acrylonitrile copolymers,[57] and nylon-66,[6] in addition to nylon-6 nanocomposites formed by in situ polymerization and melt-processing.[4,58,59]

Similar polymer structure−nanocomposite property effects are observed in the plot of yield strength vs wt % MMT shown in Figure 13. Nanocomposites formed from PA-6 exhibit dramatic improvements in yield strength with increasing clay content, while the rate of increase in yield strength in nanocomposites formed from the more aliphatic PA-11 and PA-12 matrices is less pronounced. PA-6 nanocomposites fracture prior to yielding at clay contents of ∼6 wt % and higher. On the other hand, nanocomposites based on the PA-11 and PA-12 matrices remain ductile to the high clay loadings; this is most likely related to the higher inherent ductility of the latter polymer matrices.

The elongation at break data in Figure 14 show the response of the ductility to the addition of clay. In general, increasing clay content results in a loss of

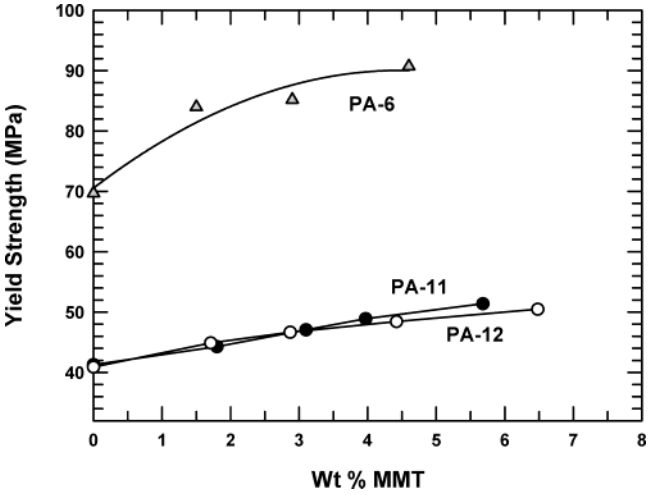

Figure 13. Effect of montmorillonite content and polyamide repeat structure on the yield strength of nanocomposites based on PA-6, PA-11, and PA-12 and the organoclay $M_3(HT)_1$.

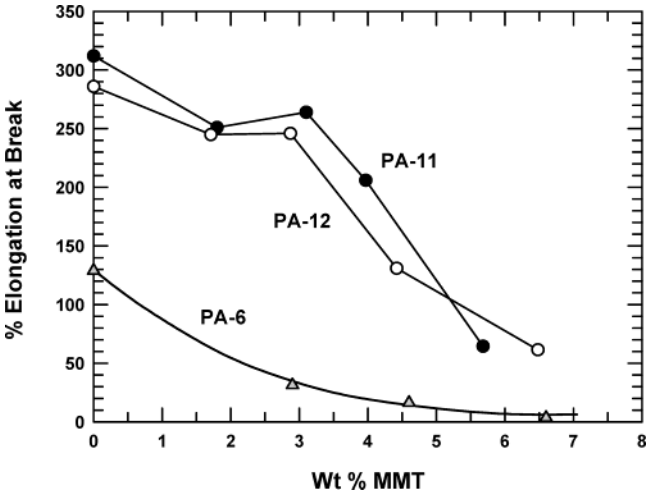

Figure 14. Effect of montmorillonite content and polyamide repeat structure on the elongation at break of nanocomposites based on PA-6, PA-11, and PA-12 and the organoclay $M_3(HT)_1$.

ductility for each polymer; however, the extent of reduction is considerably less for nanocomposites based on PA-11 and PA-12 than those based on PA-6. Similar effects are also apparent in the elongation at yield values for the three matrix materials as seen Table 3.

Overall, the tensile properties in combination with the morphological data presented earlier indicate that nylon-6 exfoliates the $M_3(HT)_1$ organoclay more effectively than do nylon-11 and -12. Since rheological and processing details were similar for all three systems, this suggest that the thermodynamic affinity between polymer and organoclay increases as the aliphatic content of the polyamide matrix decreases to cause a stronger driving force for the exfoliation of clay by the polymer. The net interaction that affects clay exfoliation consists of several components: (1) the platelet−platelet interaction which should be the same because the organoclay structure is fixed, (2) the surfactant−polymer interaction which should become increasingly less favorable the lower the aliphatic content of the polyamide,[60,61] and (3) the polymer−silicate interaction which probably becomes more favorable the more polar (or the lower the hydrocarbon content of the polyamide) the polymer is. From this simple model, we conclude that the affinity of nylon-6 for the silicate surface is

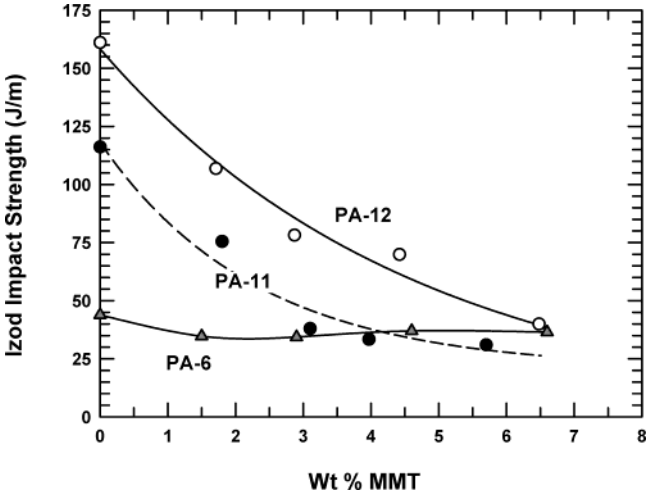

Figure 15. Effect of montmorillonite content and polyamide repeat structure on the Izod impact strength of nanocomposites formed from PA-6, PA-11, and PA-12 and the organoclay $M_3(HT)_1$.

significantly greater than that for nylon-11 or nylon-12. From a mechanical property standpoint, the modulus results, in terms of exfoliation efficiency, reflect a higher level of exfoliation for the more polar nylon-6 material, whereas the yield strengths for the different nanocomposites likely reflect both exfoliation and interfacial strength differences. This behavior is analogous to what has been observed for nylon-6 composites containing glass fibers having differing surface treatments. The yield strength of nylon-6−glass fiber composites is known to be sensitive to both the aspect ratio of the glass fiber and the chemical structure of surface treatment (or sizing), while composite modulus is relatively insensitive to the latter effect.[62]

The impact behavior of these three types of nanocomposites is shown in Figure 15. The impact strength for the neat polymers increases dramatically from nylon-6 to nylon-11 to nylon-12. Neat nylon-6 fails in a brittle manner in this test, while nylon-11 and -12 are considerably tougher; this difference is largely due to the higher ductility of the later two polymers. Adding MMT to the nylon-6 matrix has very little effect on the impact strength. On the other hand, adding MMT to PA-11 or PA-12 caused impact strength to decrease dramatically, eventually approaching a level comparable to that of corresponding nylon-6 nanocomposites. The differences in impact behavior between nylon-6 nanocomposites as compared to those based on nylon-11 and -12 can be attributed, in large measure, to how close the ductile-to-brittle transition temperature of the matrix polymer is to the ambient testing temperature. Previous studies in our laboratory have shown that the present nylon-6 has a ductile-to-brittle transition, as measured by the Izod impact test, around 55 °C.[5] Adding organoclay to this polymer results in an increase in the ductile-to-brittle transition temperature.[5] Regardless of the clay content, nylon-6-based materials exhibit brittle fractures at room temperature. On the other hand, nylon-11 and -12 in the absence of clay have ductile-to-brittle transition temperatures that are closer to room temperature, thereby resulting in considerably higher Izod impact strengths than nylon-6.[63] Adding organoclay to these matrices is also expected to increase the ductile-to-brittle transition. Thus, a viable explanation for the observed impact strengths for these nanocomposites is

that the ductile-to-brittle transition temperature for the nylon-11 and -12 matrices is increased far enough beyond room temperature to result in brittle fractures upon addition organoclay. Of course, one cannot completely rule out that less exfoliation in the nylon-11 and -12 matrices may also contribute to the drop in impact strength, owing to the larger particles acting as defects.

Conclusions

Evaluation of the effect of polyamide structure on the morphology and mechanical properties of nanocomposites has given further insight about why nylon-6 is capable of forming such well-exfoliated clay morphologies. The polarity of the repeat structure is an important factor that determines the level of interaction of the polymer with the organoclay. It appears that increasing the aliphatic content relative to nylon-6 results in a lower thermodynamic affinity between the polymer and organoclay, thus reducing the driving force for the exfoliation of clay by the polymer. Furthermore, this interaction appears to be dominated by polymer−silicate interactions, as opposed to polyamide−surfactant interactions, since the extent of clay exfoliation is higher in nylon-6 than nylon-11 and -12, despite the less favorable interaction between nylon-6 and the aliphatic tail of the organic modifier. At this point, there appears to be no conclusive evidence that the end groups of nylon-6 influence the level of clay exfoliation to the extent that the repeat structure does. Results for nanocomposites based on nylon-6 materials having capped and uncapped amine end groups reveal no significant difference in the level of clay exfoliation and mechanical reinforcement. To draw a definitive conclusion concerning end group effects, a more rigorous study involving materials whose end groups are more widely varied while having constant melt viscosity is recommended.

Acknowledgment. This work was supported by the Air Force Office of Scientific Research. We thank Mr. Randy Chapman of Southern Clay products for assistance with WAXS reflection measurements.

Appendix. Effect of Nylon-6 End Groups

The effect of nylon-6 end groups was briefly examined by comparing two polyamide materials, PA-6 and PA-6-Capped, which differ only in the concentration of amine end groups; the original intent of this study was to examine both the effect of amine and carboxylic groups on the extent of organoclay exfoliation, but the lack of a broad range of materials with differing end group balances while keeping molecular weight in the range needed for a meaningful comparison precluded this from happening. As shown earlier in Table 1, the material designated as PA 6 is a commercial grade of nylon-6 having equivalent amine and carboxylic acid concentrations of nominally 28.8 μequiv/g, while PA-6-Capped is an experimental nylon-6 material with an acid concentration comparable to PA-6, but its amine concentration is much lower due to end-capping. Figure 16 shows a plot of reflected X-ray intensity vs 2θ for nanocomposites based on PA-6 and PA-6-Capped. Both curves are relatively smooth, indicating gross separation of the clay platelets of the original organoclay. TEM photomicrographs qualitatively revealed well-exfoliated morphologies for both types of nanocomposites with no definitive difference between the two; photomicrographs

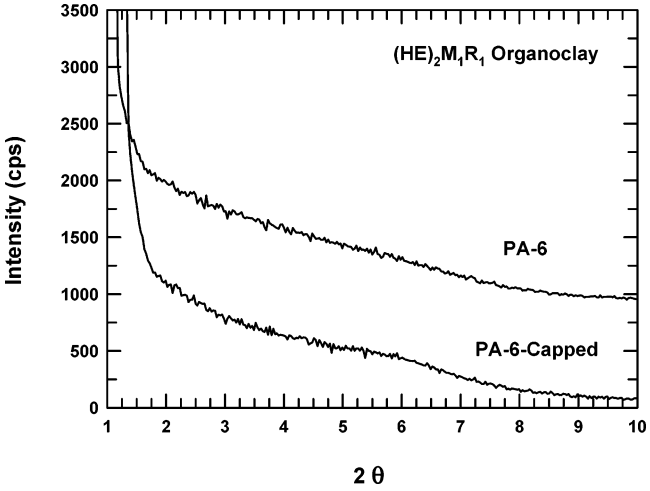

Figure 16. X-ray scans of nanocomposites based on PA-6 and PA-6-Capped and the organoclay $(HE)_2M_1R_1$. The composites contain approximately 3 wt % MMT.

Table 4. Tensile Properties for $(HE)_2M_1R_1$ Organoclay Nanocomposites Based on PA-6 and PA-6-Capped

			elongation at break (%)	
wt % MMT	modulus (GPa)	yield strength (MPa)	crosshead head speed 0.51 cm/min	crosshead head speed 5.1 cm/min
PA-6/$(HE)_2M_1R_1$ Nanocomposites				
0.0	2.75	69.7	304	129
3.2	3.92	84.9	119	27
4.6	4.59	91.3	39	25
PA-6-Capped/$(HE)_2M_1R_1$ Nanocomposites				
0.0	2.70	68.1	264	199
3.0	4.15	83.3	87	13
4.7	4.75	89.5	4.5	4.4

for the nanocomposites can be found in the Supporting Information as well as in prior publications.[8−10,49,50]

Table 4 summarizes the tensile property results for the two types of nanocomposites. Nanocomposites based on PA-6-Capped exhibit slightly higher moduli per mass of MMT than those based on PA-6, while the yield strength values for the two types of materials are nearly equivalent. Both composites also exhibit similar ductility behavior. At low rates of extension, the neat polyamides have very high elongation at break values. Adding clay to these matrices, however, results in a loss in ductility. At intermediate MMT concentrations, reasonable elongation values are maintained; however, beyond this point the values become considerably less, particularly for the nanocomposites based on PA-6-Capped. At higher test speeds, similar ductility responses are observed, but at lower absolute values.

In general, the above data provide no conclusive evidence that the type of end groups alter the extent of organoclay exfoliation by nylon-6. One might envision amine or carboxylic end groups having strong interactions with the silicate and this may be part of the picture; however, to sort this out would require access to materials with constant molecular weight or viscosity with end groups that are more widely varied, e.g., materials consisting entirely of molecules having one carboxylic end group (or amine end group) and one nonfunctional end group or no amine or carboxylic end groups at all at constant melt viscosity. Interestingly, recent nanocomposites investigations in our laboratory have revealed a significant difference in the level of exfoliation and subsequent reinforcement in nanocom-

posites based on nylon-6 as compared to those based on nylon-6,6 even under fixed thermal and rheological conditions. The differences in end groups between theses materials may be provide an explanation for this result.

Supporting Information Available: TEM photomicrographs described in the Appendix. This material is available free of charge via the Internet at http://pubs.acs.org.

References and Notes

(1) Okada, A.; Fukushima, Y.; Kawasumi, M.; Inagaki, S.; Usuk, A.; Sugiyami, S.; Kurauchi, T.; Kamigaito, O. In US Patent, Toyota Motor Co., Japan, United States, 1988.
(2) Usuki, A.; Kojima, Y.; Kawasumi, M.; Okada, A.; Fukushima, Y.; Kurauchi, T.; Kamigaito, O. *J. Mater. Res.* **1993**, *8*, 1179−1184.
(3) Christiani, B. R.; Maxfield, M. In US Patent, Allied Signal, United States, 1998.
(4) Liu, L.; Qi, Z.; Zhu, X. *J. Appl. Polym. Sci.* **1999**, *71*, 1133−1138.
(5) Cho, J. W.; Paul, D. R. *Polymer* **2001**, *42*, 1083−1094.
(6) Chavarria, F.; Paul, D. R. To appear in Polymer.
(7) Fornes, T. D.; Hunter, D. L.; Paul, D. R. *Macromolecules* **2004**, *37*, 1793−1798.
(8) Fornes, T. D.; Yoon, P. J.; Keskkula, H.; Paul, D. R. *Polymer* **2001**, *42*, 9929−9940.
(9) Fornes, T. D.; Yoon, P. J.; Keskkula, H.; Paul, D. R. *Polymer* **2002**, *43*, 2121−2122.
(10) Yoon, P. J.; Fornes, T. D.; Paul, D. R. *Polymer* **2002**, *43*, 6727−6741.
(11) Hasegawa, N.; Kawasumi, M.; Kato, M.; Usuki, A.; Okada, A. *J. Appl. Polym. Sci.* **1998**, *67*, 87−92.
(12) Hasegawa, N.; Okamoto, H.; Kato, M.; Usuki, A. *J. Appl. Polym. Sci.* **2000**, *78*, 1918−1922.
(13) Hasegawa, N.; Okamoto, H.; Kawasumi, M.; Kato, M.; Tsukigase, A.; Usuki, A. *Macromol. Mater. Eng.* **2000**, *280*, 76−79.
(14) Oshinski, A. J.; Keskkula, H.; Paul, D. R. *Polymer* **1992**, *33*, 284−293.
(15) Oshinski, A. J.; Keskkula, H.; Paul, D. R. *Polymer* **1992**, *33*, 268−283.
(16) Oshinski, A. J.; Keskkula, H.; Paul, D. R. *J. Appl. Polym. Sci.* **1996**, *61*, 623−640.
(17) Majumdar, B.; Paul, D. R.; Oshinski, A. *J. Polymer* **1997**, *38*, 1787−1808.
(18) Gelles, R.; Modic, M. J.; Kirkpatrick, J. P. *Soc. Plast. Eng., ANTEC* **1988**, *46*, 513.
(19) Glimore, D.; Modic, M. J. *Soc. Plast. Engng., ANTEC* **1989**, *47*, 1371.
(20) Modic, M. J.; Glimore, D.; Kirkpatrick, J. P. *Proc. First Int. Congr. on Compatiblization and Reactive Polymer Alloying (Compalloy '89)* **1989**, 197.
(21) Yariv, S. *Introduction to Organo-clay Complexes and Interactions*; Marcel Dekker: New York, 2002.
(22) Fornes, T. D.; Yoon, P. J.; Paul, D. R. *Polymer* **2003**, *44*, 7545−7556.
(23) Martinache, J.; Royer, J.; Siripurapu, S.; Henon, F.; Genzer, J.; Khan, S.; Carbonell, R. *Ind. Eng. Chem. Res.* **2001**, *40*, 5570−77.
(24) Majumdar, B.; Keskkula, H.; Paul, D. R. *Polymer* **1994**, *35*, 1385.
(25) Fornes, T. D.; Yoon, P. J.; Hunter, D. L.; Keskkula, H.; Paul, D. R. *Polymer* **2002**, *43*, 5915−33.
(26) Haramachi, O.-K. *Polym. Lett.* **1965**, *3*, 557−60.
(27) Kawaguchi, A.; Ikawa, T.; Fujiwara, Y.; Tabuchi, M.; Monobe, K. *J. Macromol. Sci., Phys.* **1981**, *B20*, 1−20.
(28) Rhee, S.; White, J. L. *J. Polym. Sci., Part B: Polym. Phys.* **2002**, *40*, 2624−2640.
(29) Owen, A. J.; Kollross, P. *Polym. Commun.* **1983**, *24*, 303−306.
(30) Rhee, S.; White, J. L. *J. Polym. Sci., Part B: Polym. Phys.* **2002**, *40*, 1189−1200.
(31) Dosiere, M. *Polymer* **1993**, *34*, 3160−3167.
(32) Inoue, K.; Hoshino, S. *J. Polym. Sci., Part B* **1973**, *11*, 1077.
(33) Reichert, P.; Kressler, J.; Thomann, R.; Muelhaupt, R.; Stoeppelmann, G. *Acta Polym.* **1998**, *49*, 116−123.
(34) McNally, T.; Raymond Murphy, W.; Lew, C. Y.; Turner, R. J.; Brennan, G. *P. Polymer* **2003**, *44*, 2761−2772.
(35) Aharoni, S. M. *n-Nylons, Their Synthesis, Structure, and Properties*; J. Wiley & Sons: Chichester, 1997.
(36) Arimoto, H.; Ishibashi, M.; Hirai, M.; Chatani, Y. *J. Polym. Sci., Part A* **1965**, *3*, 317−326.
(37) Holmes, D. R.; Bunn, C. W.; Smith, D. J. *J. Polym. Sci.* **1955**, *17*, 159−177.
(38) Kohen, M. I., Ed.; *Nylon Plastics Handbook*; Hanser: New York, 1995.
(39) Vogelsong, D. C. *J. Polym. Sci.* **1963**, *1*, 1055−1068.
(40) Rybnikar, F.; Burda, J. *Faserforsch. Textiltech.* **1961**, *12*, 324−331.
(41) Roldan, L. G.; Kaufman, H. S. *Polym. Lett.* **1960**, *1*, 603−608.
(42) Fornes, T. D.; Paul, D. R. *Polymer* **2003**, *44*, 3945−3961.
(43) Liu, T.; Lim, K. P.; Chauhari Tjiu, W.; Pramoda, K. P.; Chen, Z.-K. *Polymer* **2003**, *44*, 3529−3535.
(44) Halpin, J. C.; Kardos, J. L. *Polym. Eng. Sci.* **1976**, *16*, 344−352.
(45) Halpin, J. C.; Finlayson, K. M.; Ashton, J. E. *Primer on Composite Materials Analysis*; Technomic Pub. Co.: Lancaster, PA, 1992.
(46) Alexandrov, K. S.; Ryshova, T. V. *Bull. Acad. Sci. USSR, Deorphys. Ser.* **1961**, *12*, 1165−1168.
(47) McNeil, L. E.; Grimsditch, M. *J. Phys.: Condens. Matter* **1993**, *5*, 1681−1690.
(48) Van Olphen, H. *An Introduction to Clay Colloid Chemistry: For Clay Technologists, Geologists, and Soil Scientists*; Wiley: New York, 1977.
(49) Fornes, T. D.; Paul, D. R. *Polymer* **2003**, *44*, 4993−5013.
(50) Fornes, T. D.; Hunter, D. L.; Paul, D. R. *Polymer* **2004**, *45*, 2321−2331.
(51) Hine, P. J.; Rudolf Lusti, H.; Gusev, A. A. *Comput. Sci. Technol.* **2002**, *62*, 1445−1453.
(52) Wang, Z.; Pinnavaia, T. J. *Chem. Mater.* **1998**, 1820−1826.
(53) Alexandre, M.; Beyer, G.; Henrist, C.; Cloots, R.; Rulmont, A.; Jerome, R.; Dubois, P. *Macromol. Rapid Commun.* **2001**, 643−646.
(54) Manias, E.; Touny, A.; Wu, L.; Strawhecker, K.; Lu, B.; Chung, T. C. *Chem. Mater.* **2001**, *13*, 3516−3523.
(55) Reichert, P.; Nitz, H.; Klinke, S.; Brandsch, R.; Thomann, R.; Mulhaupt, R. *Macromol. Mater. Eng.* **2000**, 8−17.
(56) Liu, X.; Wu, Q. *Polymer* **2001**, *42*, 10013−10019.
(57) Stretz, H. A.; Paul, D. R. Personal communication.
(58) Kojima, Y.; Usuki, A.; Kawasumi, M.; Okada, A.; Fukushima, Y.; Kurauchi, T.; Kamigaito, O. *J. Mater. Res.* **1993**, *8*, 1185−1189.
(59) Akkapeddi, M. K. *ANTEC, Soc. Plast. Eng.* **1999**, *57*, 1619−1622.
(60) Ellis, T. S. *Macromolecules* **1990**, *30*, 998.
(61) Ellis, T. S. *Macromolecules* **1990**, *31*, 1058.
(62) Laura, D. M.; Keskkula, H.; Barlow, J. W.; Paul, D. R. *Polymer* **2002**, *43*, 4673−4687.
(63) Majumdar, B.; Keskkula, H.; Paul, D. R. *Polymer* **1994**, *35*, 1399.

MA048757O